OPEN ACCESS
IOP Publishing
Journal of Physics D: Applied Physics
J. Phys. D: Appl. Phys. **55** (2022) 105303 (7pp)
https://doi.org/10.1088/1361-6463/ac3a49

Intrinsic color centers in 4H-silicon carbide formed by heavy ion implantation and annealing

Takuma Kobayashi[1,*], Maximilian Rühl, Johannes Lehmeyer, Leonard K S Zimmermann, Michael Krieger and Heiko B Weber

Department Physik, Lehrstuhl für Angewandte Physik, Friedrich-Alexander-Universität Erlangen-Nürnberg, 91058 Erlangen, Germany

E-mail: kobayashi@prec.eng.osaka-u.ac.jp

Received 12 August 2021, revised 24 October 2021
Accepted for publication 16 November 2021
Published 1 December 2021

Abstract

We study the generation and transformation of intrinsic luminescent centers in 4H-polytype of silicon carbide via heavy ion implantation and subsequent annealing. Defects induced by the implantation of germanium (Ge) or tin (Sn) have been characterized by photoluminescence (PL) spectra recorded at cryogenic temperatures. We find three predominant but as-yet-unidentified PL signatures (labeled as DI_{1-3}) at the wavelength of 1002.8 nm (DI_1), 1004.7 nm (DI_2), and 1006.1 nm (DI_3) after high dose implantation ($> 4 \times 10^{13}$ cm^{-2}) and high temperature annealing (> 1700°C). The fact that the DI lines co-occur and are energetically close together suggest that they originate from the same defect. Regardless of the implanted ion (Ge or Sn), a sharp increase in their PL intensity is observed when the implantation damage becomes high (vacancy concentration $> 10^{22}$ cm^{-3}), indicating that the lines stem from an intrinsic defect caused by the damage. By tracking the PL signals after stepwise annealing, we examine how the overall intrinsic defects behave in the temperature range of 500 – 1800°C; the silicon vacancies formed by the implantation transform into either divacancies or antisite-vacancy pairs with annealing at about 1000°C. These spectral signatures are strongly reduced at 1200°C where the so-called TS defects are maximized in luminescence. As a final stage, the DI defects, which are most likely formed of antisites and vacancies, emerge at 1700°C. Our results provide a knowledge on how to incorporate and manipulate the intrinsic luminescent centers in SiC with ion implantation and annealing, paving the way for fully integrated quantum technology employing SiC.

Supplementary material for this article is available online

Keywords: silicon carbide, color centers, ion implantation, annealing

(Some figures may appear in colour only in the online journal)

[1] Present address: Graduate School of Engineering, Osaka University, Suita, Osaka 565-0871, Japan.
[*] Author to whom any correspondence should be addressed.

Luminescent point defects in solids are a core element for quantum technologies and nanoscale sensor applications [1, 2]. As a solid-state host, silicon carbide (SiC) is promising owing to its wide band gap and mature technology, e.g. large-wafer fabrication, isotope purification, and selective doping by ion implantation [3, 4]. Among the best studied color centers in SiC is the negatively-charged silicon vacancy (V_{Si}) [5], which acts as a near-infrared single emitter operating up to room temperature [6, 7]. Despite the lack of inversion symmetry in the crystal, the similarity of its ground and excited states makes this defect only weakly sensitive to electrostatic perturbations [8–11]. The divacancy (V_{Si}-V_C) [12] and antisite-vacancy (C_{Si}-V_C) [13] pairs are also reported as room-temperature single emitters at telecom and visible wavelengths, respectively.

To cover a wide range of applications, further exploration of luminescent defects in SiC with various photonic and spin properties is highly demanded. We opt for ion implantation because of its broad technological relevance. Implantation not only injects ions into the crystal but also damages it selectively and forms intrinsic defects. Indeed, controlled generation of intrinsic luminescent defects in SiC is achieved by proton implantation and annealing [14]. There, three sharp and temperature stable photoluminescence (PL) lines (i.e. $TS_{1–3}$ lines) are reported, which presumably originate from an intrinsic defect [14].

To find adequate future qubits and to have the chance to build future quantum technology based on SiC, a broad knowledge about different types of luminescent centers (how they can be created, manipulated, transformed, and where they originate) is essential. In that context, especially studying new PL signatures, which possibly can belong to new defects, is key to gain a full picture of the luminescent center landscape of SiC. Therefore, in the present study, we systematically investigate the effect of ion implantation and annealing on the PL signatures of SiC, using isoelectronic group-IV elements, i.e. germanium (Ge) and tin (Sn). They are implanted and produce high damage into the crystal. As a measure of the damage, the vacancy concentration calculated by *the Transport of Ions in Matter* (TRIM) [15] reaches the order of 10^{22} cm^{-3}, approaching the atomic density of SiC. After implantation, annealing at 500 – 1800°C is performed stepwise to track how the intrinsic defects are generated/annihilated during this process. In particular, we find prominent but yet unreported PL lines in the near-infrared wavelength regime, which are examined in detail.

We use high-purity semi-insulating 4H-SiC (0001) samples from Cree Inc. Figure 1(a) shows the schematic illustration of the experiment. Unless otherwise noted, epitaxial graphene is grown on the sample surface by annealing in argon (Ar) atmosphere [16] (temperature: 1675 °C) in order to eliminate the near-surface emitters [9, 14]. The fact that graphene itself does not emit PL and that its transparency is quite high (97.7%) [17] make it promising as a passivation material to study bulk luminescent centers in SiC [9, 14]. Then, room-temperature implantation of either Ge or Sn is performed at the energy of 350 keV (Ge) or 700 keV (Sn). The implantation energies are determined such that the ion concentration is maximized at the depth of about 200 nm below the sample surface. The implantation dose is varied in the range of 2×10^{13} – 1×10^{14} cm^{-2}. Figure 1(b) shows the resulting ion and vacancy concentration profiles simulated by TRIM [15]. Note that here the vacancy concentration represents the concentration of empty lattice sites which are not necessarily isolated. As shown in figure 1(b), a high quantity of damage (vacancy concentration $\sim 10^{22}$ cm^{-3}) is created by the implantation that is more prominent than the implanted ions themselves ($\sim 10^{19}$ cm^{-3}). After the implantation, samples are annealed at 500 –1800°C for 30 min. The annealing below 1000°C is performed in nitrogen, while that at or above 1000°C is performed in Ar using another furnace. For polarization measurement, a $(1\bar{1}00)$ face sample is also prepared by cutting a (0001) face wafer parallel to its primary flat and polishing its sidewall.

For measuring PL, the samples are placed inside a vacuum cryostat and cooled to cryogenic temperature (3 – 4 K) with liquid helium. To acquire spectra in a wide optical range, an incident laser with wavelength of 532 nm (Millenia Xs laser, Spectra Physics) or 785 nm (LDM785 laser, Thorlabs) is used for defect excitation. The laser beam is incident perpendicular to the sample surface. A wide field lens is used together with an objective lens to collimate the laser beam at the sample surface for ensemble measurements. The objective lens with numerical aperture of 0.65 is used for collecting the PL emission. The PL spectra are recorded either by the Andor Newton DU-920P-OE CCD camera (Newton camera) or by the Andor iDus InGaAs DU490A-1.7 camera (InGaAs camera) that are both connected to the Andor Shamrock 500i spectrograph.

Figure 2(a) shows typical PL spectra recorded for Sn-implanted samples (dose: 10^{14} cm^{-2}) as-implanted and those annealed at 500 – 1700 °C. Among the well known PL signatures (i.e. $V_{1'}$ [5, 18], V_1 [5, 18], UD_3 [19, 20], and V_2 [5, 18]), three sharp PL lines emerge after annealing at 1700 °C. These lines are labeled as DI lines ($DI_{1,\,2,\,\text{and}\,3}$) where 'DI' stands for 'damage induced'. Note that the DI lines do not show up in a non-implanted region of the very same wafer (see supplementary information available online at stacks.iop.org/JPD/55/105303/mmedia). The major PL lines observed in this study are summarized in table 1.

Figure 2(b) shows the PL spectra focusing on the DI lines for Ge- and Sn-implanted samples (dose: 10^{14} cm^{-2}) annealed at 1700 – 1800 °C. Even though a slight shift in their wavelength is observed among the measurements (within ±0.7 nm), the DI lines are observed both in the Ge- and Sn-implanted samples. These lines depend slightly differently on temperature (e.g. the intensity of DI_2 and DI_3 drops at 1750 °C, while DI_1 remains rather unaffected). Nevertheless, the facts that the lines co-arise at 1700 °C and are quite close together in energy (within 5 meV) suggest that they belong to the same microscopic defect.

It is noteworthy that further graphitization of sample surface may occur in the temperature range of 1700 – 1800°C, since it is already above the temperature where graphene is grown (1675°C). However, even after removal of the surface carbon by oxidation at 800°C for 30 min and regrowth of monolayer graphene, we confirm that the DI lines are still present. Therefore, the lines do not stem from a defect in

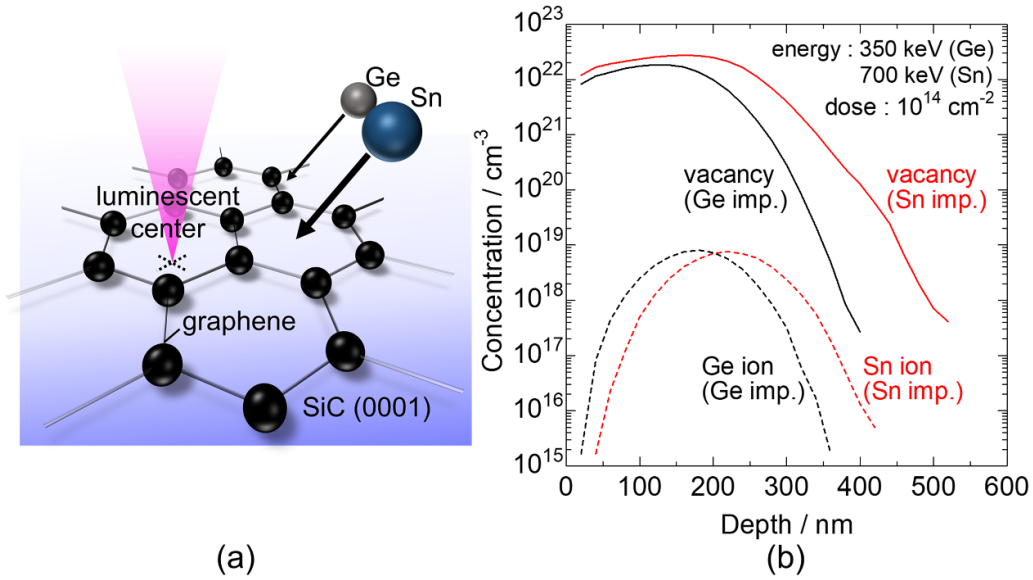

Figure 1. (a) Schematic illustration of experiment. We investigate the PL signatures of color centers in SiC induced by the implantation of either Ge or Sn. (b) Depth profiles of ion and vacancy concentrations for Ge and Sn implantations simulated by TRIM [15] (dose: 10^{14} cm^{-2}).

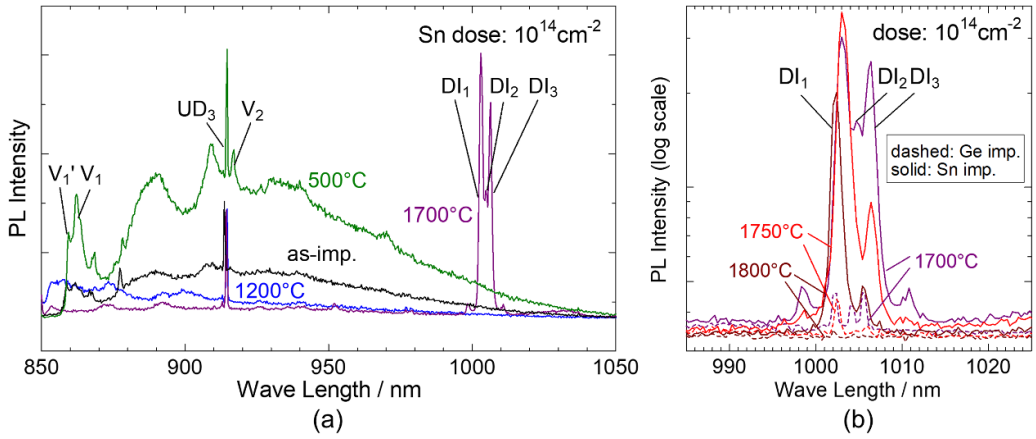

Figure 2. (a) PL spectra of Sn implanted SiC samples (dose: 10^{14} cm^{-2}), as-implanted and annealed at 500 – 1700°C. (b) Comparison of PL spectra of Ge and Sn implanted SiC samples (dose: 10^{14} cm^{-2}) annealed at 1700 – 1800°C, focusing on the DI lines. For both (a) and (b), the samples are sequentially annealed as follows: 500°C → 1000°C → 1200°C → 1400°C → 1600°C → 1700°C → 1750°C → 1800°C. The 785 nm laser is used for excitation and the spectra are recorded by the Newton camera.

surface carbon but from that in SiC. Although the DI lines appear both in Ge- and Sn-implanted samples, one may suppose that the extrinsic defects involving Ge and Sn ions may show similar PL emission. However, a theoretical calculation suggests that the dominant Ge-related defect in SiC is the Ge-on-Si antisite (Ge_{Si}) with formation energy as low as 1.47 eV, which does not form an energy level in the bandgap [24]. The same holds for carbon, where the carbon antisite (C_{Si}) has the lowest formation energy (2.61 – 2.65 eV) among the intrinsic defects in a compensated material but does not form a defect level [25]. Since Sn is a group IV element as well, a similar scenario is expected for it. Altogether, it is likely that the majority of implanted Ge or Sn ions are not active as extrinsic color centers. This is further corroborated by argon (Ar) or lead (Pb) implantation which results in the very same DI lines (see supplementary information). We conclude that the DI lines stem from an intrinsic defect.

Figure 3(a) shows the dose dependence of intensity of DI lines for Ge- and Sn-implanted samples annealed at 1750°C. Regardless of the implanted ion (Ge or Sn), a sharp increase in the PL intensity is observed at the dose of (4 – 7) × 10^{13} cm^{-2} for all three lines ($DI_{1,\,2,\,\text{and}\,3}$). The intensity of DI lines is higher in the Sn-implanted sample than for Ge (figure 2(b)). This might be attributable to the higher crystal damage induced by the Sn implantation than by Ge (figure 1(b)). Therefore, in figure 3(b), we plot the intensity of DI_1 as a function of vacancy concentration calculated by TRIM [15]. Note that the calculated vacancy concentration is that immediately after the implantation, and the recovery of damage during the following annealing steps is not

Table 1. Summary of major PL signatures observed in this study. The measured emission wavelengths ($\lambda_{emission}$) and energies ($E_{emission}$) are listed together with the emission energies in literature ($E_{emission}^{Ref.}$). All the data are collected from the sequentially annealed Sn-implanted samples (dose: 10^{14} cm^{-2}). The data for $V_{1'}$, V_{1-2}, UD_{1-3}, and DI_{1-3} are obtained using the 785 nm laser, while those for A_1, B_{2-4}, and TS_{1-3} are obtained using the 532 nm laser. All the data are those recorded by the Newton camera except for the UD_{1-2} where the InGaAs camera is used instead. Note that both the $\lambda_{emission}$ and $E_{emission}$ are extracted at the point where signal intensity is maximized. Since these quantities slightly vary among the measurements, the mean values are shown in the table. Thus, $\lambda_{emission}$ and $E_{emission}$ may contain an error of about ±0.8 nm and ±0.8 meV, respectively.

PL lines		Origin	$\lambda_{emission}$ (nm)	$E_{emission}$ (meV)	$E_{emission}^{Ref.}$ (meV)
V_1'		V_{Si} [5, 18]	859.0	1443.4	1443.6 [5]
V_1			861.8	1438.7	1439.1 [5]
V_2			916.7	1352.6	1353.0 [5]
UD_3		Unknown [19, 20]	914.4	1355.9	1355.5 [19]
UD_2	PL_4	V_{Si}-V_C [12, 21]	1078.6	1149.5	1149.3 [21]
	PL_3		1108.0	1119.0	1119.1 [21]
	PL_2		1130.7	1096.5	1096.4 [21]
	PL_1		1132.3	1095.0	1095.0 [21]
UD_1		Unknown [20, 22]	1171.0	1058.8	1059 [22]
A_1		C_{Si}-V_C [13, 23]	648.7	1911.4	1911.2 [13]
B_2			672.9	1842.5	1842.2 [13]
B_3			675.0	1836.8	1836.3 [13]
B_4			676.3	1833.4	1832.7 [13]
TS_1		Unknown [14]	769.0	1612.4	1612.7 [14]
TS_2			811.9	1527.0	1526.9 [14]
TS_3			813.2	1524.6	1524.5 [14]
DI_1		Unknown	1002.8	1236.4	—
DI_2			1004.7	1234.0	—
DI_3			1006.1	1232.4	—

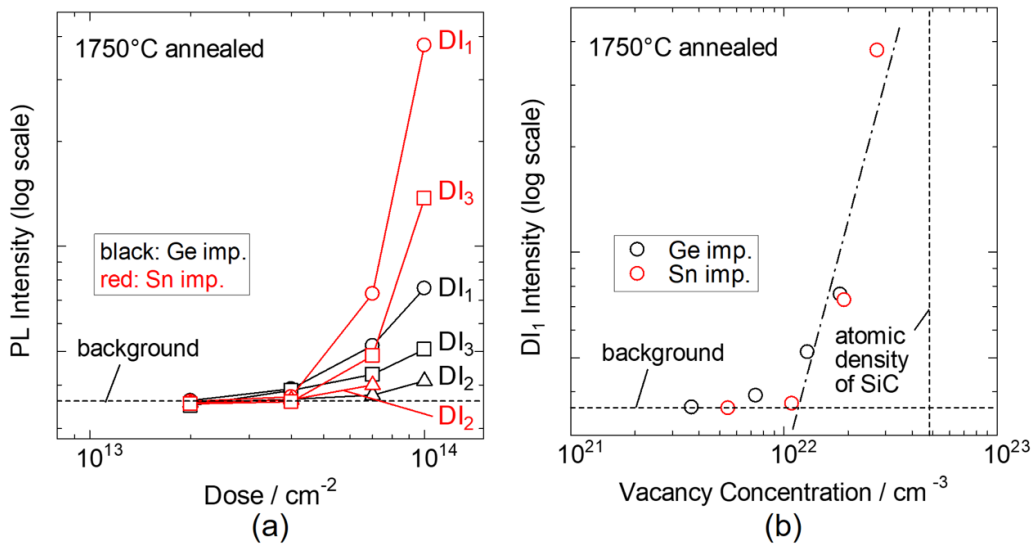

Figure 3. (a) Implantation dose dependence of PL intensity of DI lines for Ge- and Sn-implanted SiC samples (anneal temperature: 1750°C). As intensity of DI_1, DI_2, and DI_3, the maximum intensity in the energy range of 1002 – 1003 nm, 1004 – 1005 nm, and 1005 – 1006.5 nm is plotted, respectively. The intensity of DI_2 at the dose of 10^{14} cm^{-2} is not available for Sn implanted sample since it merges with DI_1. Lines connecting the data points are guides to the eye. (b) Intensity of DI_1 line for Ge- and Sn-implanted SiC samples (anneal temperature: 1750°C) as a function of initial vacancy concentration calculated by TRIM [15]. Here, the vacancy concentration denotes the maximum vacancy concentration in the sample. The intensity is extracted from the spectra in the same manner as in (a). The dot-dashed line is fitted to data with vacancy concentration above 10^{22} cm^{-3}. As a reference, the atomic density of SiC calculated from its density (3.211 g cm^{-3}) [33] is shown in the figure. For both (a) and (b), the background signal level is determined by averaging the spectrum of a Sn-implanted sample (dose: 10^{14} cm^{-2}) where there are no distinct PL lines (wavelength range: 990 – 995 nm). The 785 nm laser is used for excitation, and the spectra are recorded by the Newton camera.

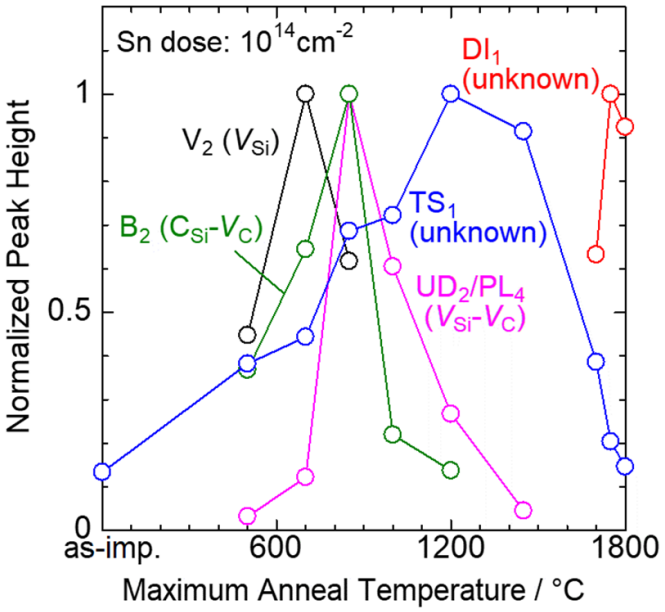

Figure 4. Anneal temperature dependence of the normalized peak height of PL lines for (presumably) intrinsic defects observed in Sn-implanted SiC samples (dose: 10^{14} cm^{-2}). To extract the peak height, each defect signal is fitted to a Lorentzian function assuming a constant background level depending on the signal. The peak height is then estimated by $A/\pi\sigma$, where A and σ are the amplitude and width of the Lorentzian, respectively. The peak height is normalized by its maximum value for each signal. The annealing is conducted sequentially as follows: 500°C → 700°C → 850°C → 1000°C → 1200°C → 1450°C → 1700°C → 1750°C → 1800°C. The 532 nm laser is used for excitation, and the spectra are recorded by the Newton camera. The solid lines connecting the data points are guides to the eye.

taken into account. As a minor point, TRIM assumes 0 K in the calculation and does not include the effect of *self-anneal* which should occur during room-temperature implantation [15]. Thus, the calculated vacancy concentration is only a measure of the initial damage in the crystal. Nevertheless, as shown in figure 3(b), a clear relationship is observed between the vacancy concentration and the intensity of DI$_1$ regardless of ion species (Ge or Sn); the intensity sharply increases when the concentration reaches the order of 10^{22} cm^{-3}. Therefore, the formation of DI lines is closely correlated to the implantation damage.

We then track the PL intensity after several annealing steps for (presumably) intrinsic defects. The results are shown in figure 4 and can be interpreted as follows; by the heavy ion implantation, high concentration of V_{Si} is initially generated. The implantation, at the same time, excessively damages the crystal and generates other types of defects, suppressing the transparency of the crystal. Moderate annealing at 500°C helps the crystal damage to recover and the signal due to isolated V_{Si} appears. The signal due to V_{Si} is maximized at 700°C. With annealing at about 1000°C, majority of V_{Si} seems to transform either into the V_{Si}-V_C or into the C_{Si}-V_C. The V_{Si}-V_C is formed when the V_{Si} and carbon vacancy (V_C) meet during the diffusive motion through the crystal [26, 27]. The $C_{Si} - V_C$ is, on the other hand, formed via the jump of a neighboring carbon atom into the V_{Si} [28, 29]. Note that a similar conversion of intrinsic defects is reported for proton-irradiated *n*-type SiC epilayers [30]. The major difference is that the creation of C_{Si}-V_C out of V_{Si} is suppressed in *n*-type material since V_{Si} possesses lower formation energies when Fermi level is located close to the conduction band [30]. The PL lines of V_{Si}-V_C and C_{Si}-V_C are reduced at 1200°C where the TS signal is maximized, suggesting that the TS defect is generated out of one of them. So far, the transformation process of defects is identical to what is reported for proton implantation, where annealing was performed up to 1600°C [14]. The crucial difference is the appearance of DI lines after annealing at 1700°C, where even the spectra signature of TS defects is strongly reduced. In principle, it should be possible to create the DI lines by proton implantation since they seem to occur due to the crystal damage (cf figure 3(b)). However, it is difficult to reach the criteria for producing these lines (i.e. vacancy concentration > 10^{22} cm^{-3}) by protons, since protons are very light; the calculated maximum vacancy concentration is 3.4 × 10^{20} cm^{-3} even for high-dose proton implantation (dose: 10^{15} cm^{-2} and energy: 350 keV). From the temperature dependence of PL signatures, a plausible process of defect transformation is suggested as follows: V_{Si} → V_{Si}-V_C or C_{Si}-V_C → TS defect (unknown) → DI defect (unknown). Thus, the DI defect is most likely a cluster of intrinsic defects (i.e. antisites and vacancies). Indeed, the clustering of C_{Si} via vacancy-assisted diffusion is predicted to occur at elevated temperatures; Assuming V_{Si} approaches C_{Si} from the left, transformation of V_{Si} → V_C-C_{Si} occurs, resulting in the creation of C_{Si} -V_C-C_{Si} complex [31]. Then V_C may recombine with the C_{Si} on the right, which enables the jump of C_{Si} into neighboring silicon sites. Thanks to the energy gain (2.2 eV) of the transformation V_{Si} → V_C-C_{Si}, the effective energy barrier for this jump is only 2.0 eV at 0 K [31]. Mediated by the above diffusive motion of C_{Si}, the clustering of antisite defects may occur with high energy gain (e.g. 7.1 eV for $Si_C(C_{Si})_4$ cluster). Vacancies (i.e. V_{Si} and V_C) may also migrate in crystal via sublattice jumps [26, 31] and form clusters. In fact, a previous theoretical study has indicated the stability of vacancy complexes [32]. There, the trivacancy (V_3; $V_C V_{Si} V_C$) and hexavacancy (V_6; $V_C V_{Si} V_C V_C V_C V_C$) are found to be relatively abundant due to their high dissociation (V_3: 1.3 eV and V_6: 1.2 eV) and attraction energies (V_3: 3.6 eV and V_6: 3.3 eV), compared to other multivacancies. Thus, a cluster of antisites and vacancies is a possible candidate for the DI defect. However, studies based on detailed analyses (e.g. electron paramagnetic resonance) and theoretical calculations are required to identify the microscopic origin of the DI defect.

Figure 5 shows the results of the polarization measurement for PL lines observed in Sn implanted samples (dose: 10^{14} cm^{-2}) annealed at 1750°C. Within ensemble measurements, no clear polarization is observed for the DI lines on (0001) face. In contrast, by measuring on (1$\bar{1}$00) face, we see that both of the DI$_1$ and DI$_3$ lines are polarized along the same direction, corroborating the model that these lines have the

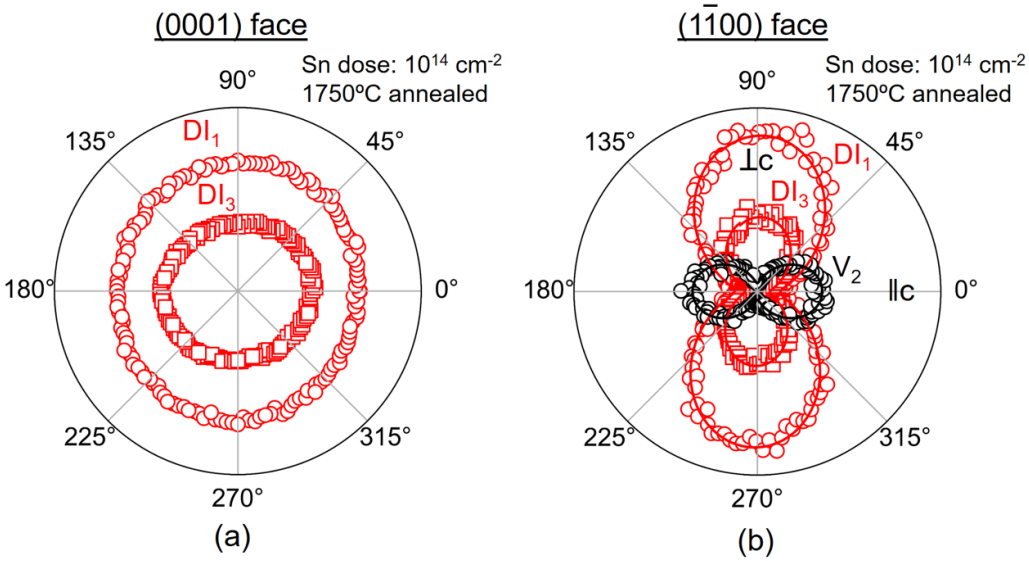

Figure 5. Polarization of the PL signatures observed in Sn implanted samples (dose: 10^{14} cm^{-2}) annealed at 1750°C: (a) (0001) face and (b) (1-100) face samples. The data are fitted with a sine function for each signature in (b). It is uncertain how the angle corresponds to actual crystal orientation in (a). In (b), the data are rotated so that 0° (or equivalently, 180°) matches the polarization of V_2 emission which should be oriented towards the crystal *c*-axis [5]. For both (a) and (b), as intensity of DI_1, DI_3, and V_2, the maximum intensity in the energy range of 1002 – 1003 nm, 1005 – 1006.5 nm, and 915.5 – 917 nm is plotted, respectively. The graphene growth process prior to the implantation was not carried out for these samples; in particular, the appropriate condition for graphene growth is not established for the (1$\bar{1}$00) face. The background counts are extracted from the signal intensity, where the background is determined by averaging one of the spectra for each sample in the region where there are no distinct PL lines (wavelength range: 990 – 995 nm). The 785 nm laser is used for excitation, and the spectra are recorded by the Newton camera.

same origin. Note that the V_2 line, which can be used as a reference to determine the crystal orientation, is detected on (1$\bar{1}$00) face even after 1750°C annealing. From the fitted sine functions, we find that the DI_1 and DI_3 lines are oriented at angles of 91.2° and 90.8°, respectively, so that of the V_2 line. Given the fact that the V_2 line is polarized *along* the crystal *c*-axis [5], the DI lines are polarized *perpendicular* to the *c*-axis.

In summary, we investigate the luminescent defects in high-purity 4H-SiC induced by heavy ion implantation and annealing. Among the previously reported PL signatures (V′, V, UD, AB, and TS), we find predominant but as-yet-unidentified signatures (DI_{1-3}) in the near-infrared wavelength regime (1002 – 1006 nm). The DI lines appear after high temperature annealing (1700°C) only in samples where high implantation damage is created (vacancy concentration > 10^{22} cm^{-3}). A clear relationship is observed between the intensity of DI lines and vacancy concentration after the implantation, indicating that the lines originate from an intrinsic defect caused by the crystal damage. By tracking the annealing temperature dependence of PL signals, we find that the signals related to the V_{Si}, V_{Si}-V_C, C_{Si}-V_C, TS, and DI defects (i.e. V_2, UD_2 (or PL_4), B_2, TS_1, and DI_1, respectively) are maximized at 700, 1000, 1000, 1200, and 1750°C, respectively. Based on this, a plausible process of defect transformation is suggested as follows; $V_{Si} \rightarrow V_{Si}$-$V_C$ or C_{Si}-$V_C \rightarrow$ TS defect $\rightarrow$ DI defect. Our results provide a guideline on how to form all of these intrinsic luminescent centers in SiC in a controlled manner, paving the way for future on-chip quantum applications using SiC.

Data availability statement

The data that support the findings of this study are available upon reasonable request from the authors.

Acknowledgments

The authors thank Michel Bockstedte for fruitful discussions. This work was supported by the Deutsche Forschungsgemeinschaft within the Project No. WE3542/10-1. T K was supported by the JSPS Overseas Research Fellowships.

ORCID iDs

Takuma Kobayashi https://orcid.org/0000-0002-2755-5079
Johannes Lehmeyer https://orcid.org/0000-0003-2041-9987
Leonard K S Zimmermann https://orcid.org/0000-0003-1595-3405
Michael Krieger https://orcid.org/0000-0003-1480-9161
Heiko B Weber https://orcid.org/0000-0002-6403-9022

References

[1] Doherty M W, Manson N B, Delaney P, Jelezko F, Wrachtrup J and Hollenberg L C L 2013 *Phys. Rep.* **528** 1
[2] Eisaman M D, Fan J, Migdall A and Polyakov S V 2011 *Rev. Sci. Instrum.* **82** 071101

[3] Kimoto T and Cooper J A 2014 *Fundamentals of Silicon Carbide Technology* (New York: Wiley)
[4] Lohrmann A, Johnson B C, McCallum J C and Castelletto S 2017 *Rep. Prog. Phys.* **80** 034502
[5] Janzén E, Gali A, Carlsson P, Gällström A, Magnusson B and Son N T 2009 *Mater. Sci. Forum* **615–617** 347
[6] Widmann M *et al* 2015 *Nat. Mater.* **14** 164
[7] Kraus H, Soltamov V A, Riedel D, Väth S, Fuchs F, Sperlich A, Baranov P G, Dyakonov V and Astakhov G V 2014 *Nat. Phys.* **10** 157
[8] Nagy R *et al* 2019 *Nat. Commun.* **10** 1054
[9] Rühl M, Bergmann L, Krieger M and Weber H B 2020 *Nano Lett.* **20** 658
[10] Udvarhelyi P, Nagy R, Kaiser F, Lee S Y, Wrachtrup J and Gali A 2019 *Phys. Rev. Appl.* **11** 044022
[11] Bathen M E, Galeckas A, Müting J, Ayedh H M, Grossner U, Coutinho J, Frodason Y K and Vines L 2019 *npj Quantum Inf.* **5** 111
[12] Koehl W F, Buckley B B, Heremans F J, Calusine G and Awschalom D D 2011 *Nature* **479** 84
[13] Castelletto S, Johnson B C, Ivády V, Stavrias N, Umeda T, Gali A and Ohshima T 2014 *Nat. Mater.* **13** 151
[14] Rühl M, Ott C, Götzinger S, Krieger M and Weber H B 2018 *Appl. Phys. Lett.* **113** 122102
[15] Ziegler J F, Biersack J P and Littmark U 1985 *The Stopping and Range of Ions in Solids* (Oxford: Pergamon)
[16] Emtsev K V *et al* 2009 *Nat. Mater.* **8** 203
[17] Gonçalves P A D and Peres N M R 2016 *An Introduction to Graphene Plasmonics* (Hackensack: World Scientific Publishing)
[18] Baranov P G, Bundakova A P, Soltamova A A, Orlinskii S B, Borovykh I V, Zondervan R, Verberk R and Schmidt J 2011 *Phys. Rev.* B **83** 125203
[19] Wagner M, Magnusson B, Chen W M and Janzén E 2002 *Phys. Rev.* B **66** 115204
[20] Magnusson B and Janzén E 2005 *Mater. Sci. Forum* **483–485** 341
[21] Magnusson B, Son N T, Csóré A, Gällström A, Ohshima T, Gali A and Ivanov I G 2018 *Phys. Rev.* B **98** 195202
[22] Kalabukhova E N, Savchenko D V, Greulich-Weber S, Bulanyi M F, Omelchenko S A, Khmelenko O V, Gorban A A and Mokhov E N 2006 *Mater. Sci. Forum* **527–529** 651
[23] Steeds J W 2009 *Phys. Rev.* B **80** 245202
[24] Krieger M, Rühl M, Sledziewski T, Ellrott G, Palm T, Weber H B and Bockstedte M 2016 *Mater. Sci. Forum* **858** 301
[25] Kobayashi T, Harada K, Kumagai Y, Oba F and Matsushita Y I 2019 *J. Appl. Phys.* **125** 125701
[26] Gali A, Bockstedte M, Son N T, Umeda T, Isoya J and Janzén E 2006 *Mater. Sci. Forum* **527–529** 523
[27] Son N T *et al* 2006 *Phys. Rev. Lett.* **96** 055501
[28] Bockstedte M, Mattausch A and Pankratov O 2004 *Phys. Rev.* B **69** 235202
[29] Bockstedte M, Mattausch A and Pankratov O 2003 *Phys. Rev.* B **68** 205201
[30] Karsthof R, Bathen M E, Galeckas A and Vines L 2020 *Phys. Rev.* B **102** 184111
[31] Rauls E, Frauenheim T, Gali A and Deák P 2003 *Phys. Rev.* B **68** 155208
[32] Iwata J I, Shinei C and Oshiyama A 2016 *Phys. Rev.* B **93** 44
[33] Gomes de Mesquita A H 1967 *Acta Crystallogr.* **23** 610